Journal of The Electrochemical Society

OPEN ACCESS

Vat Orange 11—Based Organic Cathode Material for High Rate Rechargeable Magnesium Battery

Journal of The Electrochemical Society, 2020 **167** 070561

Vat Orange 11—Based Organic Cathode Material for High Rate Rechargeable Magnesium Battery

Tripathy Debashis,[1] H. M. Viswanatha,[1] M. N. K. Harish,[2] and S. Sampath[1,z]

[1]*Department of Inorganic and Physical Chemistry, Indian Institute of Science, Bangalore, India*
[2]*Department of Chemistry, Acharya Institute of Technology, Soldevanahalli, Bangalore, India*

Mg-ion batteries are of immense interest owing to their dendrite free chemistry, low cost and high energy density and often comparable to the existing Li-ion batteries. Organic molecules as electrodes, are well-explored in alkali metal ion batteries as they are less expensive, environment friendly and amenable to redox potential-tuning. But these molecules are rarely used for secondary Mg-ion batteries and they continue to attract attention. In the present studies, an organic dye, vat orange 11, is explored as a cathode material for non-aqueous secondary Mg-ion battery in different electrolytes. The electrolyte with salt-controlled dissolution approach turns out to be very good in terms of capacity recovery with long cycle life. It shows an excellent rate performance up to a discharge current of 4000 mA g^{-1} with high cycling stability (1000 cycles at 500 mA g^{-1} current density). Further, high capacity and high rate performance are observed using a non-nucleophilic electrolyte based on an ionic liquid. The possible mechanism of Mg^{2+} uptake is studied using ex situ FTIR spectroscopy that shows a transformation between carbonyl (–C=O) and enolate (–C=O$^-$) functional groups during charge-discharge cycles. The present studies initiate the use of vat-based dye molecules in rechargeable Mg-ion batteries.

 [DOI: 10.1149/1945-7111/ab8827]

Manuscript submitted April 2, 2020. Published April 21, 2020. *This paper is part of the JES Focus Issue on Challenges in Novel Electrolytes, Organic Materials, and Innovative Chemistries for Batteries in Honor of Michel Armand.*

Supplementary material for this article is available online

Alternate high energy storage systems other than Li-ion batteries are required to satisfy the increasing energy demand for high energy-related applications, for example, in electric vehicles. In this direction, magnesium can be useful particularly because of its high theoretical capacity (volumetric capacity- 3833 mAh cm^{-3} and gravimetric capacity-2205 mAh g^{-1}).[1] The fact that metallic Mg is less reactive to oxygen and water under ambient conditions and dendrite-free deposition, makes it an ideal candidate for a safe battery system. Moreover, it is abundant and relatively less-expensive than the battery materials based on Li.[2] Rechargeable Mg-ion batteries have gained attention after Aurbach et al. reported the prototype Mg-ion battery using Grignard reagent based electrolyte $Mg(AlCl_2EtBu)_2$/tetrahydrofuran (THF) and chevrel phase Mo_6S_8 electrode.[3] Since then various electrolytes and electrode materials have been proposed for rechargeable Mg-ion battery. Among the known electrode materials, only very few can store Mg reversibly. The best-known material, Mo_6S_8 is limited by its low theoretical capacity (128 mAh g^{-1}) and low voltage ($\sim$1.3 V). A major issue with Mg-ion battery is the interaction of Mg^{2+} ion with the host lattice. Its high charge density makes the diffusion process very slow.[4] Even if Mg^{2+} ions are inserted into the host lattice, the extraction process is difficult and leads to irreversible structural changes, poor capacity recovery as observed in the case of α-MnO_2.[5] Recently, cation deficient TiO_2 with a reversible capacity of $<$160 mAh g^{-1} and moderate discharge voltage are proposed for reversible intercalation of Mg^{2+}.[6] To avoid the sluggish kinetics of Mg^{2+} ions, a hybrid system with the electrolyte containing both Mg^{2+} and Li^+ is proposed where Mg^{2+} intercalation or Mg-Li co-intercalation is expected at the cathode and Mg stripping/platting at the anode.[7]

Organic molecules are not only sustainable but also environmentally benign. Organic materials have a distinct advantage as compared to the inorganic counterparts since the ion storage property basically depends on the interaction of functional groups and metal ion.[8] Especially, the compounds containing carbonyl groups are known for their structural stability. They coordinate with the monovalent metal ion or interact with multivalent ions by intermolecular interaction.[9] Organic molecular systems also offer flexibility for designing high voltage batteries by simply introducing electron-withdrawing functional groups.[9,10] Though there have been extensive reports on the use of organic molecules in alkali metal ion batteries,[9,11,12] there are only a handful of reports on their use for rechargeable Mg-ion batteries. Very often, anthraquinone and benzoquinone derivatives,[1,2,13–19] are reported to be useful. The redox-active sites in organic molecules can accommodate Mg^{2+} ions electrochemically and reversibly through weak intermolecular forces (electron transfer). Various molecules and their polymers like 2,5-dimethoxy-1,5-benzoquinone (DMBQ),[13,14,18,19] poly(anthraquinone) (PAQ),[17] poly(anthraquinonylsulfide) (PAQS),[15,17] poly(hydrobenzoquinonylbenzoquinonyl-sulfide) (PHBQS),[16] poly(2,2,6,6-tetramethylpiper- idinyloxy-4-ylmethacrylate)(PTMA),[20,21] pyromellitic dianhydride (PMDA) based polyimides,[22] naphthalene-hydrazine polyimide (NP),[23] perylenediimide-ethylenediamine (PDI-EDA) and polytriphenylamine (PTPAn)[24] etc have been explored as electrode materials in secondary, non-aqueous, organic Mg-based batteries. Recently, poly(hexylviologendichloride) (PHV-Cl) and pyrene-based polymer poly(hexaazatrinaphtha- lene) (PHATN) have been studied in non-aqueous Mg batteries.[25,26] Mai et al. have used 3,4,9,10-perylene tetracarboxylic dianhydride (PTCDA) as a cathode in PhMgCl-$AlCl_3$ (APC) electrolyte and the performance is reported to be improved by controlling the dissolution of the organic electrode material by using a hybrid electrolyte system consisting of APC and LiCl/NaCl/KCl.[27] Although some of the organic electrodes show a capacity of $>$150 mAh g^{-1}, cyclability is an issue and most of the reported materials suffer from poor cyclability.

Herein, we report a non-aqueous, rechargeable Mg-ion battery using vat orange 11 as a cathode material in APC-based electrolytes and a non-nucleophilic ionic liquid-based electrolyte. Vat orange 11 that contains three conjugated anthraquinone groups can be extracted from plants or synthesized in a laboratory. These dyes are generally used as colorant for fabrics. Vat dye based organic molecules (vat green 8, vat brown BR and vat olive T) and their graphene composites have been used as cathodes for Li-ion batteries.[28] To the best of our knowledge, there is no report on Mg-ion batteries that use any vat dye as an electrode material. It is observed that these molecules are very promising and capacity of $\sim$80 mAh g^{-1} at 100 mA g^{-1} current density is observed for a fairly large number of

[z]E-mail: sampath@iisc.ac.in

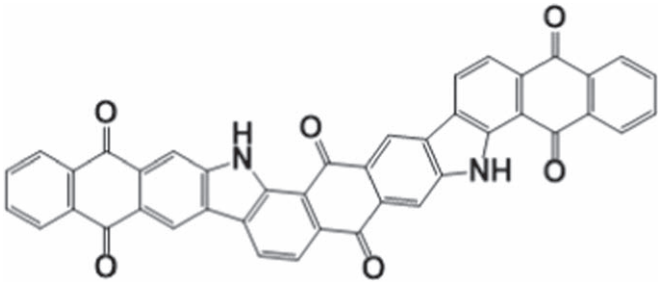

Scheme 1. Structure of Vat orange 11.

cycles. High current capability can also be achieved. The mechanism of Mg^{2+} ion storage is investigated by ex situ FTIR spectroscopy.

Experimental

Materials and electrolyte preparation.—Commercial vat orange 11 was obtained from Atul Limited, India and used without further purification. Tetrahydrofuran (THF), Phenyl magnesium chloride (PhMgCl) (2M in THF), lithium chloride (LiCl), anhydrous magnesium chloride [$MgCl_2$] and magnesium bis(hexamethyldisilazane) [$Mg(HMDS)_2$] were purchased from Sigma Aldrich, USA and anhydrous aluminum chloride ($AlCl_3$, purity 99.99%) was obtained from Alfa Aesar, USA. N-methyl-N-propyl-piperidinium bis(trifluoromethane sulfonyl)imide [$PP_{13}TFSI$] was purchased from IoLiTec, Germany. N-methyl pyrrolidine (NMP) and activated carbon (AC) were purchased from SD fine chemicals, India. The solvent, THF was dried over 3 Å molecular sieves for three days prior to use. Mg foils were procured from Goodfellow, UK. The surface of Mg foil was cleaned using various fine grade emery sheets (grade 800, 600, 200) and wiped with tissue paper before use.

The APC electrolyte was prepared according to a method reported in the literature.[29] Briefly, $AlCl_3$ was dissolved in THF and an appropriate quantity of PhMgCl was added slowly followed by stirring the solution to obtain 0.4 M 2PhMgCl-$AlCl_3$. A required amount of LiCl was added to the as-prepared APC electrolyte to prepare APC-LiCl electrolyte. The ionic liquid based electrolyte was prepared by following a reported method.[30] Briefly, a solution of $Mg(HMDS)_2$ (1.25 mmol, 431.35 mg)] in 5 ml THF was prepared to which anhydrous $MgCl_2$, (5 mmol, 476 mg) was added. Finally, $PP_{13}TFSI$ (2.5 ml) was added to the solution and kept at least 48 h for stirring to get a colourless electrolyte [$Mg(HMDS)_2$-4$MgCl_2$/2THF-$PP_{13}TFSI$ or $MMTP_{13}TFSI$].

Characterization.—The vat orange 11 dye was characterized by NMR, IR and powder X-ray diffraction (XRD) techniques. The

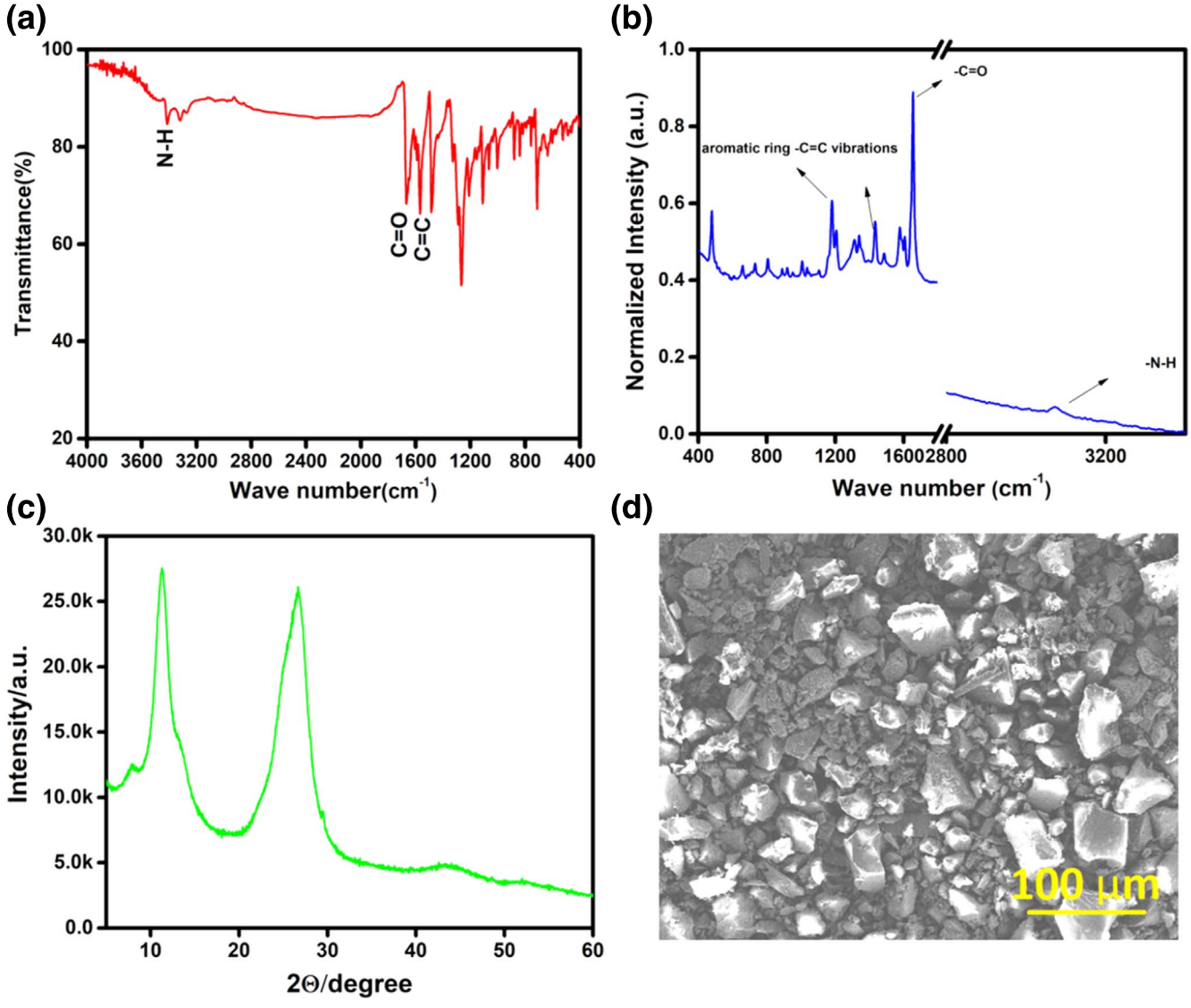

Figure 1. (a) FTIR spectrum, (b) FT Raman spectrum, (c) XRD pattern and (d) SEM image of pure vat orange 11.

solid-state ^{13}C NMR was recorded using JEOL (ECX 400) NMR spectrometer. The Fourier transform infrared (FTIR) spectrum was obtained using Perkin Elmer FTIR spectrometer and the FT Raman spectrum was obtained using Brucker FT Raman spectrometer with 1064 nm laser source. XRD measurements were carried out using Philips analytical (PAN Analytical) X-ray BV diffractometer (The Netherlands) with Cu Kα (λ = 1.5418 Å) as the X-ray source. Morphology of the samples were obtained using field emission scanning electron microscopy (FESEM, Carl Zeiss ultra 55).

Electrochemical measurements.—All the electrochemical measurements were carried out in coin-type cells (CR2032). The cells were assembled, and the electrolyte was prepared inside an Argon filled glove box (Jacomex) with moisture and oxygen level below 1 ppm. Mg was used as a negative electrode and glass microfiber (Whatman) as a separator. 0.4 M 2PhMgCl-$AlCl_3$ (APC), APC with 1M LiCl (APC-LiCl) and $MMTP_{13}TFSI$ were used as electrolytes. The positive electrodes were prepared by coating the slurry made of vat orange 11, acetylene black or activated carbon and polyvinylidene fluoride (PVDF) in 5:4:1 weight ratio respectively with few drops of N-methyl pyrrolidine (NMP) on carbon paper and then vacuum dried at 80 °C for 12 h. Electrochemical experiments were carried out using Biologic, France and Arbin, USA instruments. Cyclic voltammetry (CV) and electrochemical impedance spectroscopy (EIS) experiments were carried out using Biologic instrument and galvanostatic charge-discharge experiments were carried out in Arbin instrument, USA. All the EIS were recorded in the frequency range of 100 kHz–0.1 Hz with an amplitude of 10 mV.

Result and Discussion

The structure of vat orange 11 is confirmed by solid-state ^{13}C NMR (Fig. S1 is available online at stacks.iop.org/JES/167/070561/mmedia) as it is not soluble in any solvent and the peaks observed correspond to carbonyl carbons, and carbons due to the aromatic rings. The chemical shift value for carbonyl (–C=O) carbon is ~183.72 ppm. The chemical shift values for carbons of aromatic rings lies between 110 and 140 ppm. The chemical shift values observed in the ranges, 20−60 ppm and 200−240 ppm are due to spinning bands. The FTIR spectrum (Fig. 1a) reveals peaks around 1667 and 1655 cm^{-1} that correspond to the carbonyl (–C=O) double bond stretching vibrations. A peak around 1565 cm^{-1} is due to the –C=C double bond stretching vibrations of the aromatic rings. A small broad peak at 3080 cm^{-1} corresponds to –N–H stretching vibration. The –C–H bond vibrations are observed between 850 and 750 cm^{-1}. The Raman spectrum as shown in Fig. 1b confirms the structure. The highest intense peak around 1655 cm^{-1} corresponds to ν (C=O) and the peak around 3070 cm^{-1} corresponds to ν (N–H) vibrations. The peaks around 1183 and 1433 cm^{-1} are due to aromatic ring –C=C vibrations. Sharp peaks in the X-ray diffraction (XRD) pattern (Fig. 1c) reveal that the as-extracted, solid material is highly crystalline in nature. The diffraction peaks around 12° and 28° 2θ values are likely to be due to π-π stacking of the aromatic moieties. The morphology (Fig. 1d) shows a granular-like structure with sizes ranging from hundreds of nanometers to a few hundreds of micrometers.

Activated carbon shows a capacitive behaviour coupled with good stability, conductivity, wide pore size distribution and it is a preferred current collector material for energy storage devices. It possesses low energy density and high-power density that can take care of slow ion transport and provide good rate performance.[31] This has been realized in Li-ion battery with $LiFePO_4$ as the active material. Balducci et al. observed improved rate capability and conductivity along with a good performance at high current rates when activated carbon is used in place of super P carbon.[32] So, activated carbon can be used to improve the rate capability of rechargeable Mg-ion batteries. In the present studies, both acetylene black and activated carbon were used as conducting carbon for the electrode preparation.

Electrochemical studies have been carried out in coin cell configuration with Mg foil anode in combination with vat orange 11 in acetylene black or activated carbon separately as cathodes and APC as the electrolyte. Figure S2 shows the cyclic voltammograms of vat orange 11 electrode with acetylene black in the potential range of 1.2−2.4 V for the first five cycles at 0.1 mV s^{-1} scan rate. In the cathodic scan, the first cycle shows a board peak around 1.4 V which vanishes in subsequent cycles and this peak is possibly related to activation of the electrode material. A broad oxidation peak around 2.05 V along with a small peak at 2.2 V are observed in the anodic scan. In the second cycle, additional small reduction peaks at potentials <2.0 V are observed while the oxidation peak remains almost at the same potential but with lower peak current. The peaks remain unchanged in subsequent cycles. The cyclic voltammograms are very similar to that reported for PAQ[17] wherein redox peaks due to quinone reduction/oxidation are present. Similar, cathodic and anodic peaks are observed when the voltammogram is recorded at different scan rates, from 0.1−1.0 mV s^{-1} as shown in Figs. 2a and 2b for the electrodes acetylene black and activated carbon respectively. Increase in the peak currents with a slight change in the peak position as a function of scan rate indicates a fairly reversible redox process. The logarithmic plots of peak current vs. scan rates (log i vs. log ν) as shown in Fig. S3 give the slope, b. The slope of log i vs. log ν plot reflects whether the electrochemical process is diffusion-controlled or capacitive in nature. The process is diffusion-controlled when b = 0.5 and capacitive when b = 1. For the electrode with acetylene black, the b values are 0.57 (peak 1) and 0.93 (peak 2) while 0.76 (peak 1) and 1.1 (peak 2) with activated carbon. It indicates a slightly high capacitive contribution of activated carbon as compared to that with acetylene black.

The charge-discharge characteristics reveal that the vat orange 11 electrodes can deliver a reversible capacity of ~35 and 80 mAh g^{-1} with acetylene black and activated carbon respectively at the current density of 100 mA g^{-1} for 100 cycles as shown in Figs. 2c and 2d. The capacities offered by acetylene black and activated carbon alone are very low and shown in Fig. S4. The galvanostatic charge-discharge profiles of the cells with acetylene black and activated carbon are shown in Figs. 2e an 2f. A flat plateau observed for the first discharge analogous to the very first cycle in the voltammogram. After the first cycle, a decrease in polarization is observed with the plateau region becoming short. Initial discharge capacities of 172 and 260 mAh g^{-1} are observed with acetylene black and activated carbon respectively with voltage plateau around 1.5 V. This high capacity in the first cycle may be due to some compositional changes in the material that can be observed from the loss of crystallinity and changes in the IR spectrum as well as red coloration of the separator (Fig. S5) after charge-discharge at 100 mA g^{-1} current density. The capacities are calculated based on the mass of vat orange 11 used in the electrode. The discharge capacity decreases in the intial cycles and subsequently remains constant. With activated carbon, the capacity stabilizes at ~80 mAh g^{-1} for over 100 cycles which is similar to the theoretical capacity (~83 mAh g^{-1} considering two-electron process) for vat orange 11. Figures 2g and 2h show the rate performance of the vat orange 11 electrodes at various current densities. The reversible capacity decreases with increasing discharge current density and capacities of 55, 42, 20 and 10 mAh g^{-1} at current densities of 100, 200, 500 and 1000 mA g^{-1} respectively are observed for the electrode with acetylene black. However, electrode with activated carbon can deliver a capacity of ~26 mAh g^{-1} even at a very high current density of 2000 mA g^{-1}. Hence, the rate performance as well as the capacity values at high current densities are improved for activated carbon electrode as compared to that of acetylene black electrode. The long-term cycling stability test of the electrode was carried out at 500 mA g^{-1} current density and is shown in Fig. 3. It is stable up to 1000 cycles with ~98% of Coulombic efficiency and 67% of the capacity retention at the end of 1000 cycles.

Salt-controlled dissolution process is employed in which LiCl is used along with APC electrolyte to inhibit the dissolution of vat

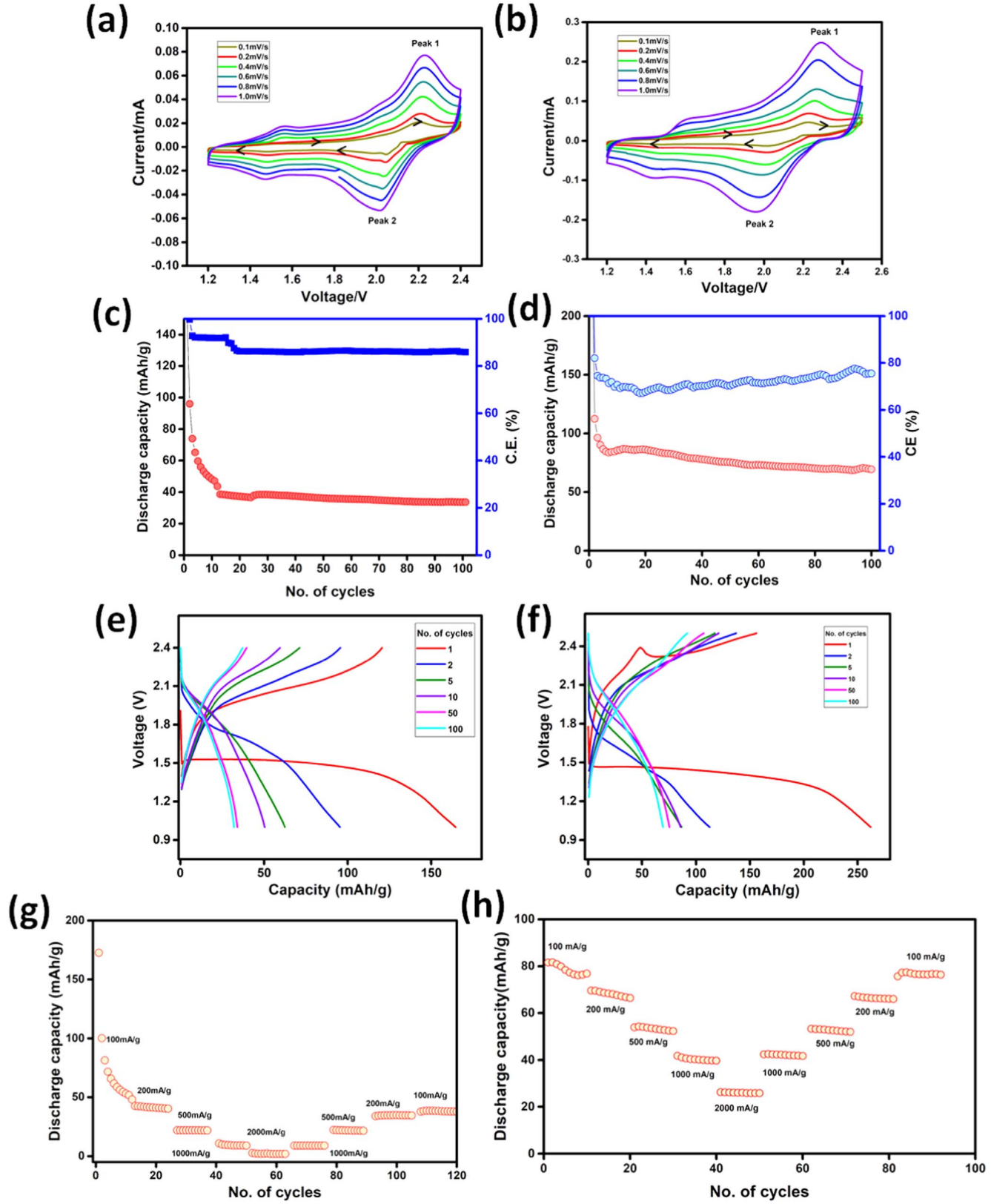

Figure 2. Cyclic voltammograms of vat orange 11 electrode at different scan rates from 0.1 to 1.0 mV s^{-1} with (a) acetylene black (OCV = 1.82 V)and (b) activated carbon (OCV = 1.88 V), cycling performance of the electrode at 100 mA g^{-1} current density with (c) acetylene black and (d) activated carbon, (e) and (f) corresponding galvanostatic charge-discharge profiles, rate performance of electrode with (g) acetylene black and (h) activated carbon at different current densities in APC electrolyte.

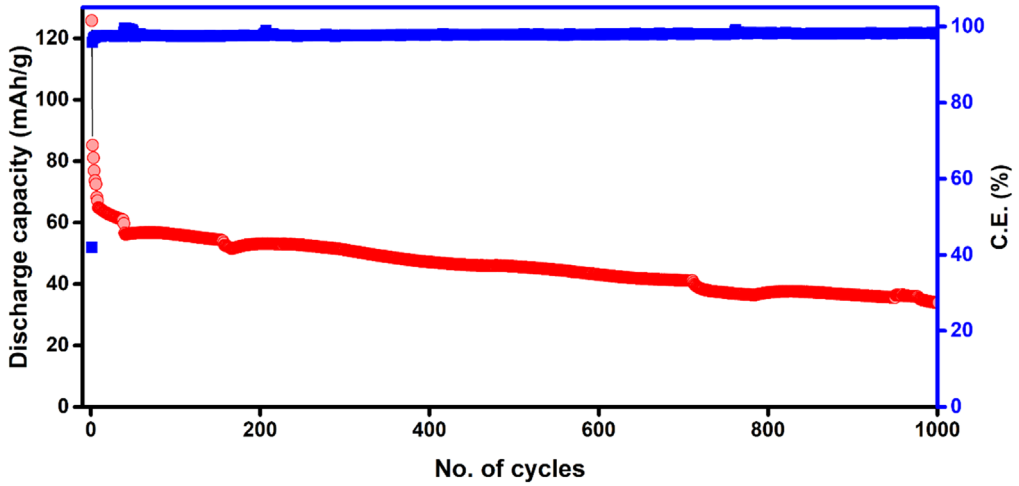

Figure 3. Long term cycling stability of the vat orange 11 electrode with activated carbon at 500 mA g^{-1} current density in APC electrolyte.

orange 11. Similar studies have been carried out by Mai et al. using PTCDA as cathode for rechargeable Mg-ion battery where the addition of salts like LiCl, NaCl and KCl to APC electrolyte supressed the dissolution of the organic cathode and high rate capability up to 500 mA g^{-1} with good cycling stability of 200 cycles at 200 mA g^{-1} current density are observed.[27] The dissolution experiments are carried out in APC and APC-LiCl electrolytes at different time intervals. The optical images (Fig. S6) show a decrease in the dissolution of vat orange 11 in the APC-LiCl electrolyte as compared to that observed in pure APC electrolyte. Further, the dissolution inhibition is confirmed from the FTIR spectra of the electrolytes. As shown in Fig. S7, there is no noticeable change in the transmittance of APC-LiCl electrolyte unlike APC electrolyte after 24 h. of soaking. In the electrolyte without LiCl, the change in intensities of the peaks present at ~1346, 1420, 1462, 1480 and 1823 cm^{-1} reflect the dissolution of vat orange 11. The presence of colour in the separator after charge-discharge process is faint (as shown in Fig. S9) in the electrolyte with LiCl as compared to the electrolyte without LiCl. Hence, it is confirmed that the dissolution of vat orange 11 in the electrolyte is relatively suppressed. It is likely that the dissolution of the lithiated dye is decreased when the concentration of the Li^+ ions in the electrolyte is increased.

Based on the above observations, electrochemical investigations are carried out using 1 M LiCl in the APC electrolyte. Figure 4a shows the voltammograms obtained at various scan rates from 0.1 to 1.0 mV s^{-1} in the potential range of 1.0−2.5 V vs Mg/Mg^{2+}. A set of redox peaks is observed like in the earlier studies but with increased peak currents possibly due to increased conductivity of the electrolyte. The "b" values obtained from the logarithmic plots of peak current vs. scan rate (Fig. S8) indicate a mixed process. The rate performance of vat orange 11/activated carbon electrode as shown in Fig. 4b reveals significant improvement and the capacity vales are also enhanced as compared to the values observed in pure APC electrolyte. An initial discharge capacity of 246 mAh g^{-1} is observed at the current density of 100 mA g^{-1} and a stable capacity of ~80 mAh g^{-1} is obtained. The long-term cycling stability is carried out at a current density of 500 mA g^{-1}. As shown in Fig. 4c, it is nearly stable up to 1000 cycles with ~98% of Coulombic efficiency. After the initial decay, the capacity remains almost constant. At the end of 1000 cycles, nearly 95% capacity retention is observed. Still the red coloration of separator (Fig. S9) is observed after charge-discharge cycles (100 cycles at 100 mA g^{-1} current density) reveals possibilities of some chemical changes during charge-discharge cycles. This is possibly due to the supressed dissolution of the vat orange 11 in the APC-LiCl electrolyte which is similar to the observations made by Mai et al. for PTCDA electrode in APC electrolyte with different salts as mentioned earlier.[27]

The Nyquist plots before and after charge-discharge experiments of vat orange 11/activated carbon electrode in APC-LiCl electrolyte are shown in Fig. 5 and the corresponding equivalent circuit diagram as well as the expanded plots in the high frequency range are shown in the inset of Fig. 5. Similar impedance behaviour has been reported for Li-ion batteries using various vat dyes[28] and other inorganic systems as well.[33] Various electrical elements used in the equivalent circuits are, internal resistance (R_{in}), constant phase element (Q) in parallel with the resistance due to surface passivation (R_{sp}) and the double layer capacitance (C_{dl}) in parallel with the Warburg diffusion element (W) due to Mg^{2+} ion diffusion and the charge transfer resistance (R_{ct}). Initially, the arc of semicircle is large indicating a very low charge transfer rate. After the charge-discharge cycles, the overall cell impedance as well as the arc of the semicircle is reduced that reflects facile Mg^{2+} ion uptake. The R_{ct} value is decreased from 471 ohm before charge-discharge experiment to 45.5 ohm after the charge-discharge cycles. This indicates that the decreased interfacial resistance after the charge-discharge cycle possibly leads to enhanced cycling and good rate performance. The diffusion constant values are calculated from the EIS data to be $2.528*10^{-14}$ cm^2 s^{-1} and $4.97*10^{-14}$ cm^2 s^{-1} before and after the charge-discharge experiments.

Although the dissolution problem can be avoided to certain extent, the resulting battery cannot be considered as a pure Mg-ion battery. Hence, a non-nucleophilic electrolyte based on ionic liquid ($MMTP_{13}TFSI$) is used to study the performance of vat orange 11/acetylene black electrode. Figure 6a shows the galvanostatic charge-discharge profiles of vat orange 11/acetylene black at 100 mA g^{-1} current density. Unlike APC-based electrolytes, well defined plateaus are observed for both discharge and charge processes in this electrolyte. Discharge and charge capacities of ~81 and 83 mAh g^{-1} respectively, are observed for the first cycle and the polarization is found to be very high. After the first cycle, decrease in polarization is observed. Even after 100 cycles, the plateaus are observed clearly, and the curves overlap indicating a highly reversible process. The cycling performance of the electrode at a current density of 100 mA g^{-1} is shown in Fig. 6b. Initially for few cycles, an activation-type process is observed which could be due to the magnesiation and subsequent oxidation after which the capacity decrease is fairly small and yields a value of ~80 mAh g^{-1}.

The electrode is cycled at various current densities to evaluate the rate performance as shown in Fig. 6c. The $MMTP_{13}TFSI$ electrolyte shows higher capacity and stable performance as compared to APC-based electrolytes. This indicates that although we can limit the dissolution of the electrode material by using LiCl, it is not possible

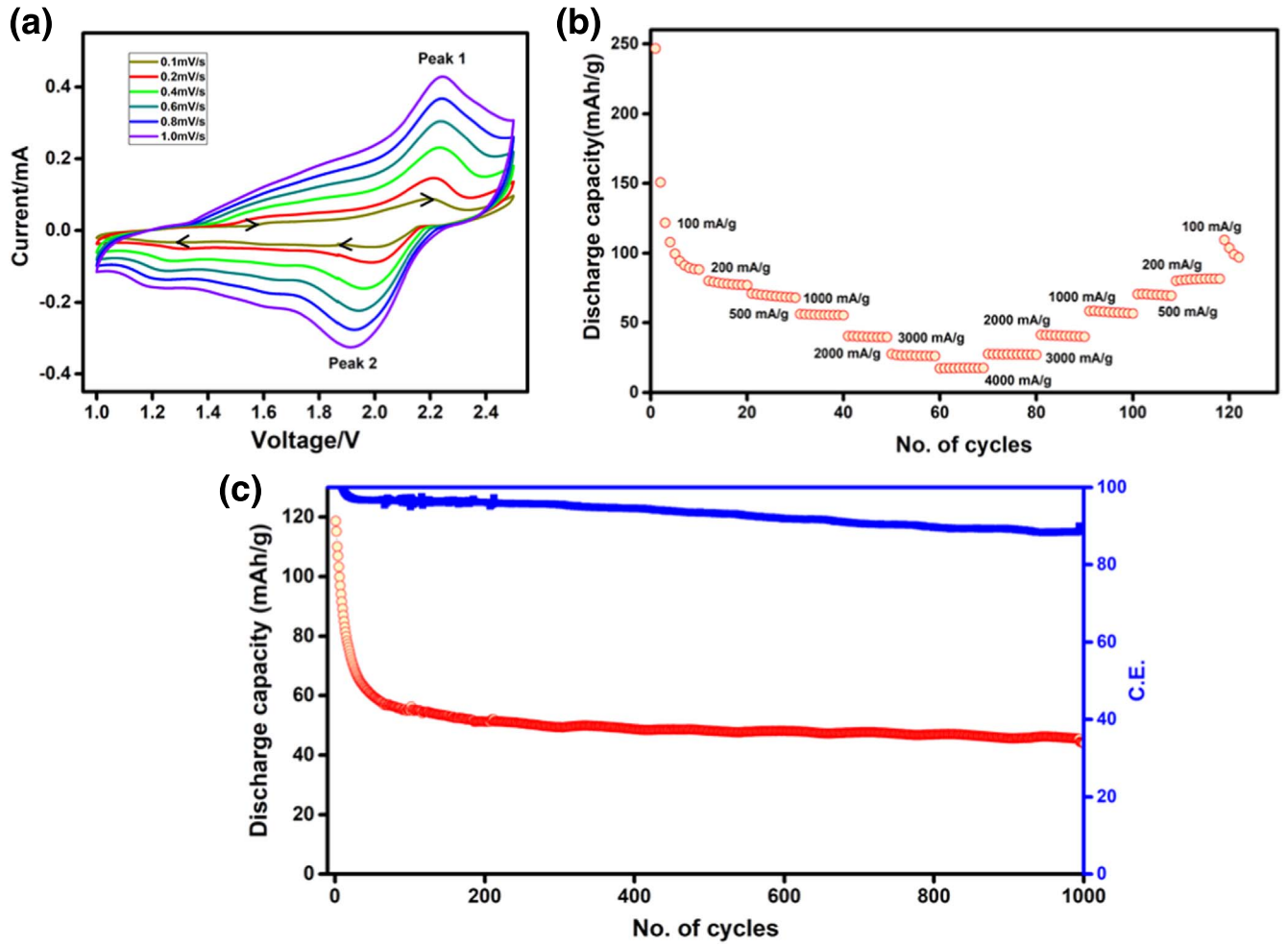

Figure 4. (a) Voltammetry curves of vat orange 11/activated carbon electrode at different scan rates from 0.1 to 1.0 mV s^{-1} (OCV = 1.88 V) in the potential range of 1.0–2.5 V, (b) rate performance at different current densities from 100 to 4000 mA g^{-1} in APC-LiCl electrolyte.

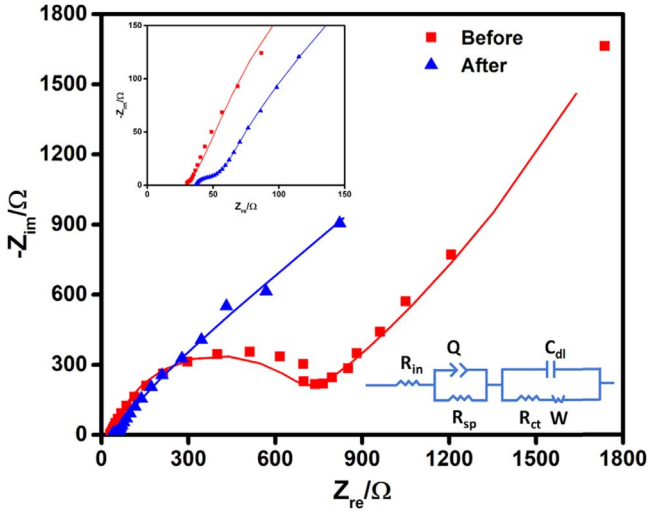

Figure 5. Nyquist plots for vat orange 11/activated carbon electrode in APC-LiCl electrolyte before and after the charge-discharge cycles (inset: equivalent circuit and the expanded plot).

to avoid the nucleophilic nature of APC affecting the performance of the material. There is a change in the composition of the material followed by a decrease in performance.

In the $MMTP_{13}TFSI$ electrolyte, the electrode can deliver a capacity of ~15 mAh g^{-1} even at a high current density of 1000 mA g^{-1} and stable capacity values are observed at all current densities. Further, the capacity value is regained when the cell is cycled back to 100 mA g^{-1} current density after cycling at high current values, indicating a highly reversible process. The cell is cycled at 500 mA g^{-1} current density to obtain information on the cycling stability (Fig. 6d). A stable capacity of ~25 mAh g^{-1} is obtained upto 500 cycles. Close to the end of 500 cycles, the cell retains ~63% of the initial capacity which is comparable to that of PAQS where 70% capacity retention has been reported after 100 cycles at a current density of 112 mA g^{-1}.[17] The obtained results with the non-nucleophilic electrolyte is comparable to the performance of anthraquinone-based systems reported in the literature for Mg-ion battery as presented in Table I. The performance of all the organic electrodes reported till date for Mg-based rechargeable batteries is given in Table SI1.[2,13–27,30,34,35]

The mechanistic details on the uptake/release of magnesium ions during charge-discharge is investigated using ex situ FTIR spectra recorded after different charge-discharge cycles at 100 mA g^{-1} current density. The obtained FTIR spectra are shown in Fig. 7. The pristine electrode shows bands around 1667 and 1655 cm^{-1} and 1565 cm^{-1} that correspond to –C=O and –C=C stretching vibrations respectively. In the case of vat 11 orange, the first discharge shows a broad peak centred at ~1642 cm^{-1} and the peaks due to carbonyl (–C=O) double bonds have disappeared. A new peak assigned to enolate ($–C=O^-$) group appears at ~1388 cm^{-1}. The peak assigned to –C=C double bonds disappears after the first

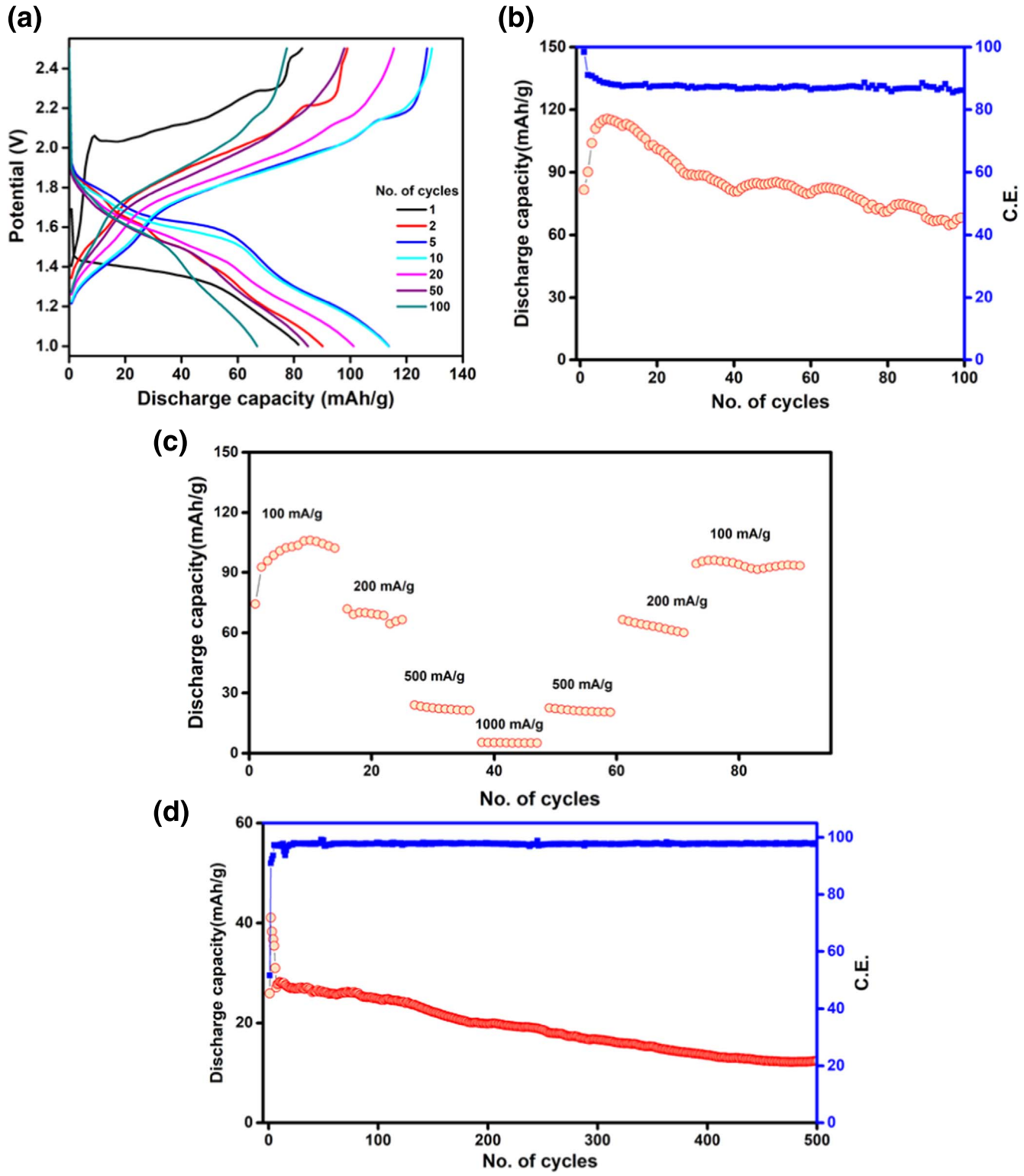

Figure 6. Cycling performance of the vat orange 11/acetylene black electrode at 100 mA g^{-1} current density, (b) corresponding galvanostatic charge-discharge profiles, (c) rate performance at different current densities and (d) cycling stability at 500 mA g^{-1} current density in $MMTP_{13}TFSI$ electrolyte.

discharge indicating the involvement of –C=C double bonds of the aromatic ring in the magnesium uptake. The above results indicate that the carbonyl (–C=O) double bonds acquire partial single bond character through resonance and get converted to enolate ($–C=O^{-}$) groups during discharge. In the subsequent charging process, the peaks due to –C=O and –C=C double bonds recover to the original positions though they are broadened as compared to the original band shapes. During second discharge, the band corresponding to –C=O double bond is found to be shifted and the band associated with –C=C double bond disappears along with the evolution of $–C=O^{-}$ peak. These results indicate that the magnesiation and demagnesiation process follows a transformation mechanism between carbonyl and enolate groups. Similarly, the IR spectra after 10th, 20th, 50th and 100th charge-discharge cycles show that the

Table I. Comparison of vat orange 11 electrode performance with anthraquinone-based organic compounds for rechargeable Mg-ion battery.

Electrode	Electrolyte	Counter electrode	No. of cycles_capacity @current density	Potential window (V)	References
Poly(anthraquinoyl) sulfides	MHCC MACC MTCC	Mg Mg powder	80 cycles_**60 mAh g^{-1}** @50 mA g^{-1} 100 cycles_**40 mAh g^{-1}** @50 mA g^{-1} 100 cycles_**50 mAh g^{-1}** @ 50 mA g^{-1}	0.5−2.5	15
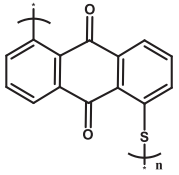 PAQS 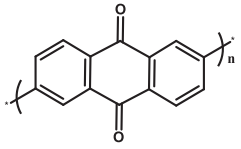 26PAQ 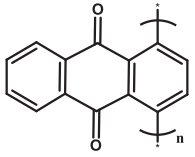 14PAQ	$Mg(HMDS)_2$-$4MgCl_2$ /THF	Mg	100 cycles_**30 mAh g^{-1}** @112 mA g^{-1} 100 cycles_**100 mAh g^{-1}** @130 mA g^{-1} 100 cycles_**100 mAh g^{-1}** @130 mA g^{-1} 1000 cycles_**60 mAh g^{-1}** @520 mA g^{-1}	0.5−2.5	17
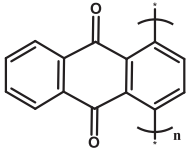 14PAQ	$Mg(TFSI)_2$-$MgCl_2$/glyme $MgCl_2$-$AlCl_3$/glyme	Mg	500 cycles_**100 mAh g^{-1}** @260 mA g^{-1} 500 cycles_**50 mAh g^{-1}** @260 mA g^{-1}	0.5−2.5	18
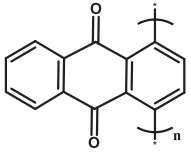 14PAQ	$Mg(TFSI)_2$/diglyme	Mg	100 cycles_**150 mAh g^{-1}** @130 mA g^{-1}	0.8−2.0	19
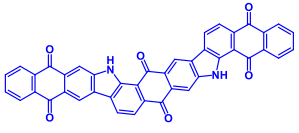	$Mg(HMDS)_2$-$MgCl_2$/THF and $PP_{13}TFSI$	Mg	100 cycles_**80 mAh g^{-1}** @100 mA g^{-1} 500 cycles_**26 mAh g^{-1}** @500 mA g^{-1}	1.0−2.5	This work

(MHCC-[Mg_2Cl_3-6THF] [$HMDSAlCl_3$] in THF, MACC- $MgCl_2$–$AlCl_3$ in THF, MTCC- $MgCl_2$–$Mg(TFSI)_2$ in a mixture of THF and glyme).

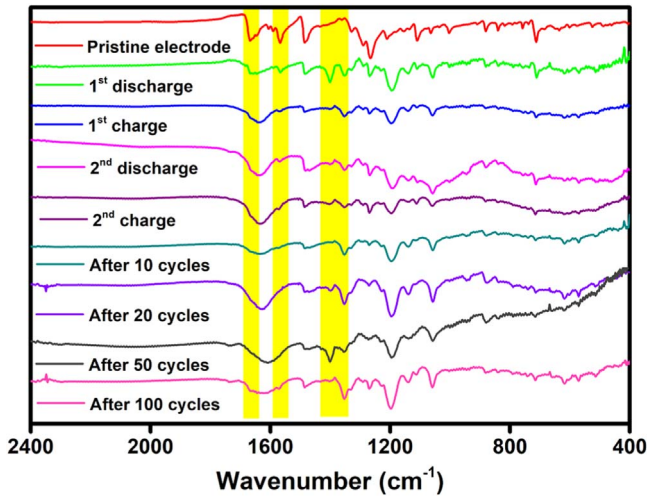

Figure 7. Ex-situ FTIR spectra of vat orange 11 electrode at different charge-discharge cycles showing the functional group transformation.

material is intact and involves the functional group transformation. The theoretical capacity of the organic molecule is ~83 mAh g^{-1} based on two-electron transfer and the values are ~166 and 249 mAh g^{-1} for 4 and 6 electron processes respectively. Experimentally observed capacity value (~80 mAh g^{-1}) indicates that vat 11 orange is involved in a two electron transfer process during charge-discharge process. The possible reaction sequence during discharge-charge process is given in the supporting information (Scheme 1).

Summary

In summary, vat orange 11 is successfully used as a cathode for secondary non-aqueous Mg-ion battery. Vat orange 11 shows a moderate reversible capacity and rate performance in APC electrolyte. Excellent rate performance, high capacity, and high cycling stability are achieved by using activated carbon instead of acetylene black as conducting carbon along with vat orange 11 in APC-LiCl electrolyte. It delivers a stable capacity of ~50 mAh g^{-1} at a high current density of 500 mA g^{-1} for 1000 cycles. Finally, a Mg-ion battery with non-nucleophilic electrolyte and vat orange 11/acetylene black is realized which shows a high capacity of ~80 mAh g^{-1} at 100 mA g^{-1} current density. The magnesiation and demagnesiation mechanism as probed by ex situ FTIR measurements shows the involvement of functional group transformation between carbonyl (–C=O) and enolate (–C=O^-) moieties.

Acknowledgments

We would like to thank V. R. Sai Ganesh, General Manager, Atul Limited, Thane, Maharastra, India for supplying sample of vat orange 11. Debashis Tripathy thanks IISc. for providing the fellowship. DST, New Delhi is acknowledged for research funding.

ORCID

Tripathy Debashis https://orcid.org/0000-0002-6458-6157
S. Sampath https://orcid.org/0000-0003-0777-2161

References

1. H. Senoh, H. Sakaebe, H. Tokiwa, M. Uchida, H. Sano, M. Yao, and T. Kiyobayashi, *ECS Trans.*, **69**, 33 (2015).
2. B. Pan, D. Zhou, J. Huang, L. Zhang, A. K. Burrell, J. T. Vaughey, Z. Zhang, and C. Liao, *J. Electrochem. Soc.*, **163**, A580 (2016).
3. D. Aurbach, Z. Lu, A. Schechter, Y. Gofer, H. Gizbar, R. Turgeman, Y. Cohen, M. Moshkovich, and E. Levi, *Nature*, **407**, 724 (2000).
4. P. Canepa, G. Sai Gautam, D. C. Hannah, R. Malik, M. Liu, K. G. Gallagher, K. A. Persson, and G. Ceder, *Chem. Rev.*, **117**, 4287 (2017).
5. C. Ling, R. G. Zhang, T. S. Arthur, and F. Mizuno, *Chem. Mater.*, **27**, 5799 (2015).
6. T. Koketsu et al., *Nat. Mater.*, **16**, 1142 (2017).
7. Y. W. Cheng, H. J. Chang, H. Dong, D. Choi, V. L. Sprenkle, J. Liu, Y. Yao, and G. S. J. Li, *Mater. Res.*, **31**, 3125 (2016).
8. S. Muench, A. Wild, C. Friebe, B. Haupler, T. Janoschka, and U. S. Schubert, *Chem. Rev.*, **116**, 9438 (2016).
9. J. Xie and Q. Zhang, *Small*, **15**, 1805061 (2019).
10. J. E. Bachman, L. A. Curtiss, and R. S. Assary, *J. Phys. Chem. A*, **118**, 8852 (2014).
11. S. Lee, G. Kwon, K. Ku, K. Yoon, S. K. Jung, H. D. Lim, and K. Kang, *Adv. Mater.*, **30**, 1704682 (2018).
12. A. Mauger, C. Julien, A. Paolella, M. Armand, and K. Zaghib, *Materials*, **12**, 1770 (2019).
13. H. Sano, H. Senoh, M. Yao, H. Sakaebe, and T. Kiyobayashi1, *Chem. Lett.*, **41**, 1594 (2012).
14. H. Senoh, H. Sakaebe, H. Sano, M. Yao, K. Kuratani, N. Takeichi, and T. Kiyobayashia, *J. Electrochem. Soc.*, **161**, A1315 (2014).
15. J. Bitenc, K. Pirnat, T. Bancic, M. Gaberscek, B. Genorio, A. R. Vitanova, and R. Dominko, *Chem. Sus. Chem.*, **8**, 4128 (2015).
16. J. Bitenc, K. Pirnat, G. Mali, B. Novosel, A. R. Vitanova, and R. Dominko, *Electrochem. Comm.*, **69**, 1 (2016).
17. B. Pan et al., *Adv. Energy Mater.*, **6**, 1600140 (2016).
18. J. Bitenc, K. Pirnat, E. Zagar, A. R. Vitanova, and R. Dominko, *J. Power Sources*, **430**, 90 (2019).
19. H. Dong, Y. Liang, O. Tutusaus, R. Mohtadi, Y. Zhang, F. Hao, and Y. Yao, *Joule*, **3**, 782 (2019).
20. S.-Y. Ha, Y.-W. Lee, S. W. Woo, B. Koo, J.-S. Kim, J. Cho, K. T. Lee, and N.-S. Choi, *ACS Appl. Mater. Interfaces*, **6**, 4063 (2014).
21. Q. Chen, Y.-N. Nuli, W. Guo, J. Yang, J.-L. Wang Jiu, and Y.-G. Guo, *Acta Phys. -Chim. Sin.*, **29**, 2295 (2013).
22. X. Fan, F. Wang, X. Ji, R. Wang, T. Gao, S. Hou, J. Chen, T. Deng, X. Li, and L. Chen, *Angew. Chem.*, **130**, 7264 (2018).
23. T. Bančič, J. Bitenc, K. Pirnat, A. K. Lautar, J. Grdadolnik, A. R. Vitanova, and R. Dominko, *J. Power Sources*, **395**, 25 (2018).
24. D. Lu, H. Liu, T. Huang, Z. Xu, L. Ma, P. Yang, P. Qiang, F. Zhanga, and D. Wu, *J. Mater. Chem. A*, **6**, 17297 (2018).
25. A. B. Ikhe, N. Naveen, K.-S. Sohn, and M. Pyo, *Electrochim. Acta*, **283**, 393 (2018).
26. M. Mao et al., *Angew. Chem. Int. Ed.*, **58**, 17820 (2019).
27. L. Cui, L. Zhou, K. Zhang, F. Xiong, S. Tan, M. Li, Q. An, Y.-M. Kang, and L. Mai, *Nano Energy*, **65**, 103902 (2019).
28. W. Ai et al., *Adv. Funct. Mater.*, **27**, 1603603 (2017).
29. O. Mizrahi, N. Amir, E. Pollak, O. Chusid, V. Marks, H. Gottlieb, L. Larush, E. Zinigrad, and D. Aurbach, *J. Electrochem. Soc.*, **155**, A103 (2008).
30. Y. Wang, Z. Liu, C. Wang, Y. Hu, H. Lin, W. Kong, J. Ma, and Z. Jin, *Energy Storage Mater.*, **26**, 494 (2019).
31. Y. Guan, J. Shen, X. Wei, Q. Zhu, X. Zheng, S. Zhou, and B. Xu, *Electrochim. Acta*, **294**, 148 (2019).
32. N. Bockenfeld, T. Placke, M. Winter, S. Passerini, and A. Balducci, *Electrochim. Acta*, **76**, 130 (2012).
33. H. Manjunatha, T. V. Venkatesha, and G. S. Suresh, *J. Solid State Electrochem.*, **16**, 1941 (2012).
34. Y. NuLi, Z. Guo, H. Liu, and J. Yang, *Electrochem. Commun.*, **9**, 1913 (2007).
35. J. Tian, D. Cao, X. Zhou, J. Hu, M. Huang, and C. Li, *ACS Nano*, **12**, 3424 (2018).